



A synergistic damage mechanics based multiscale model for composite laminates subjected to multiaxial strains



John Montesano, Chandra Veer Singh*

Materials Science and Engineering, University of Toronto, 184 College St., Suite 140, Toronto M5S 3E4, Canada

ARTICLE INFO

Article history:

Received 29 May 2014

Received in revised form 24 November 2014

Available online 12 January 2015

Keywords:

Synergistic damage mechanics

Multiscale modeling

Micromechanics

Multiaxial strain

Multidirectional laminates

Stiffness degradation

ABSTRACT

A multiscale model based on synergistic damage mechanics is developed for predicting the elastic response of symmetric composite laminates containing matrix cracks in plies of multiple orientations, and subjected to an arbitrary multiaxial strain state. On the micro-mechanical scale, the proposed multiscale modeling approach invokes three-dimensional finite element analysis to characterize the multiaxial damage state within the cracked multidirectional laminate, and evaluate damage constants required in the damage constitutive model. These damage constants capture the ply constraint effects acting on the surface displacements of the developed matrix cracks in all off-axis and on-axis plies. The representative volume element describing the applied multiaxial stress state within the laminate is developed through finite element models using periodic boundary conditions, which are necessary to accurately represent the physical problem. The developed micromechanical models also allow for prediction of the laminate's shear deformation response. The model is shown to accurately capture the nonlinear stiffness degradation exhibited by cross-ply, quasi-isotropic and angle-ply laminates containing matrix cracks in multiple plies and subjected to various multiaxial stress states. The prediction results are validated by available experimental data and compared with independent three-dimensional finite element calculations. The multiscale model can easily be implemented into a commercial finite element software package in order to predict stiffness degradation in composite structures. This will provide a means to predict the integrity and durability of these structures, and ultimately lead to damage-tolerant designs.

© 2015 Elsevier Ltd. All rights reserved.

1. Introduction

For a wide range of practical structural applications, orienting the plies of composite laminates along multiple directions is required to meet specific directional strength and stiffness requirements. A key issue with the design of multidirectional laminates is that their microstructure is quite complex, leading to a complex stress state upon load-

ing. In these laminates, local matrix cracks tend to develop in multiple directions simultaneously as the structure is progressively loaded (Tong et al., 1997). These subcritical matrix or ply cracks, which are contained within the individual plies and are usually oriented along the respective fiber directions, do not cause immediate failure but rather accumulate during loading. This consequently leads to a complex three-dimensional problem as cracks in multiple orientations evolve simultaneously with differing rates and densities (Singh and Talreja, 2009). The difficulty of the problem increases further when the laminates are subjected to complex multiaxial stress or strain states representing the real application of composite structures. In

* Corresponding author. Tel.: +1 (416) 946 5211; fax: +1 (416) 978 4155.

E-mail addresses: john.montesano@utoronto.ca (J. Montesano), chandraveer.singh@utoronto.ca (C.V. Singh).

such situations, the multidirectional crack state will be subjected to additional crack driving stress components, which will ultimately alter the resulting material behavior. Since practical structures are subjected to multiaxial loading, or more generally local multiaxial stress states, it is important for corresponding prediction models to account for the influence of these stress states on matrix cracking. This is essential for accurately predicting the integrity and durability of practical structures, and for performing progressive failure analysis. This is in fact a main focus of the third world-wide failure exercise (WWFE-III) conducted by Kaddour et al. (2013), in which the evolution of subcritical damage and its effect on the mechanical response of composite laminates is considered. If a multi-axial progressive damage model can be integrated with a non-destructive evaluation (NDE) technique, a real-time structural health monitoring tool can be developed. This will effectively lead to the design of safer and more cost-effective composite structures.

With respect to its undamaged state, the behavior of a laminate in the presence of subcritical matrix cracks is altered, and therefore the local damage state must be considered in prediction models in order to accurately capture this inelastic material behavior and to determine the ultimate material strength or stiffness (Varma et al., 2001). A reduction in the laminate stiffness properties is one of the main outcomes of the evolving damage state. Currently, there are no rigorous and comprehensive prediction tools to assess the response of such multidirectional laminates undergoing progressive damage development in the form of ply cracks in multiple-oriented plies under multiaxial loading. Current designs are far too conservative since they do not account for the evolving damage state during the design process, and as a result the laminate capabilities are not fully utilized. A number of models have been developed in recent years that attempt to predict stiffness degradation in composite laminates resulting from ply cracking. Many analytical models were developed with this purpose, including the shear-lag model by Highsmith and Reifsnider (1982), the variational models by Hashin (1985) and Naim (1989), and the self-consistent approximation by Dvorak et al. (1985). Most of these models only consider cross-ply laminates and are not suitable for practical scenarios involving multidirectional laminates consisting of a mix of both on-axis and off-axis plies.

Additional models that correlate matrix cracking with stiffness degradation are those based on the principles of continuum damage mechanics (e.g., Allen et al., 1987; Ladeveze and LeDantec, 1992; Talreja, 1985). The main advantage with such models is that the effects of particular damage modes can be directly incorporated into the constitutive equations through the use of damage tensors. However, a key drawback of continuum-based damage models is their reliance on extensive experimental testing for calibrating the material damage parameters. In order to alleviate this problem, Talreja (1996) proposed a synergistic damage mechanics (SDM) approach that combines the strengths of micromechanics and continuum mechanics to produce a versatile multi-scale methodology. The methodology relies on computational micromechanics, in lieu of experimental testing, to calibrate the material damage

parameters. Following this approach, a predictive model for off-axis ply cracking in multidirectional laminates was later developed by Singh and Talreja (2009, 2010) to predict the behavior of laminates containing multidirectional ply cracks. The model has also been applied to conduct several test cases of the WWFE-III exercise (Singh and Talreja, 2013). To understand the underlying concepts and the details of the SDM methodology, the reader is referred to Talreja and Singh (2012).

It should be noted that only a few models reported in the literature account for multiaxial loading, or more generally the local multiaxial stress states inherent in multidirectional laminates. Recent studies have been reported in which local multiaxial stresses and their influence on ply crack initiation and development are accounted for (e.g., McCartney, 1998; Mayugo et al., 2010; Vyas and Pinho, 2012; Laurin et al., 2013; Chamis et al., 2013; Kashtalyan and Soutis, 2013; Flatscher et al., 2013). Nonetheless, most of the reported models either limit their application to unidirectional or cross-ply laminates, or to multidirectional laminates containing only cracks in one transverse direction. Furthermore, they simplify the inherent complex boundary value problem by assuming that a two dimensional geometric representation of ply cracks is sufficient. Such a two dimensional representation of the problem does not accurately capture the local crack behavior and the surrounding stress state, and thus a three dimensional solution becomes necessary when multiple ply cracks are present (Singh and Talreja, 2009). In addition to the above, many of the indicated models rely on extensive experimental data for their calibration, which is seen as another limitation. Finally, a number of these models do not consider the evolution of discrete damage modes and the influence of the constraining effect between the adjacent plies in a laminate.

The focus of this study is to improve the capabilities of the aforementioned multiscale SDM approach by including multiaxial capabilities in the prediction methodology. Specifically, emphasis is placed on expanding the capability of the micromechanics computations in order to account for multiaxial effects on stiffness degradation, and to include the capability of predicting shear modulus degradation. The long-term goal is to predict damage evolution in practical composite components subjected to multiaxial stresses (see Montesano and Singh, 2015), and the current study is the first step towards this goal. A brief overview of the SDM methodology is presented in the subsequent sections, with emphasis on the laminate constitutive laws and the micromechanical computational models. The prediction results for three types of multidirectional laminates (cross-ply, quasi-isotropic and angle-ply) is then presented along with a rigorous discussion. Finally, the main findings of the study are outlined in the conclusions.

2. Synergistic damage mechanics model

2.1. Damage characterization in multidirectional laminates subjected to multiaxial strains

Consider a multidirectional laminate consisting of unidirectional on-axis, off-axis and transverse plies as shown

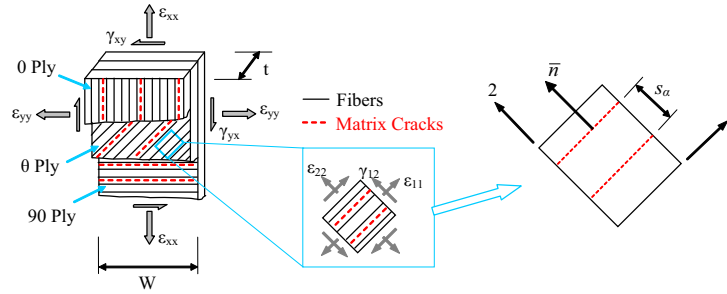


Fig. 1. An RVE of a damaged multidirectional laminate subjected to a two-dimensional multi-axial strain state – transformed strain components are shown for the θ ply only.

in Fig. 1, where off-axis orientations are denoted by θ . When subjected to quasi-static multi-axial loading, ply cracks may initiate and multiply simultaneously in plies with different orientations. Experimental observations indicate that these sub-critical cracks span the ply thickness and are oriented along the fiber direction (see Fig. 1). It must be noted that ply cracks are in fact single cracks that result from the rapid coalescence of smaller matrix and fiber–matrix interface cracks within the ply. Under multi-axial loading conditions, it is important that the prediction model accounts for the transformed strain components (i.e., ε_{11} , ε_{22} , and γ_{12} in Fig. 1) since these are the main crack driving mechanisms.

In order to characterize a particular damage state, consider the continuum body of an inhomogeneous material as shown in Fig. 2. In the presence of widespread microscopic damage, the effective laminate material properties can be determined by defining a representative volume element (RVE) of the laminate with volume V as shown in Fig. 1. Assuming there are N different damage entities for a given damage mode, α , in the RVE, the damage state for a particular damage mode can be represented by a second-order tensor as, Talreja (1994):

$$D_{ij}^{(\alpha)} = \frac{1}{V} \sum_{k_x} (d_{ij})_{k_x} \quad (1)$$

where $k_x = 1, 2, \dots, N$. Assuming that the influence of cracks is governed by Mode I only (i.e., normal crack opening), then the damage tensor is defined by, Singh and Talreja (2009):

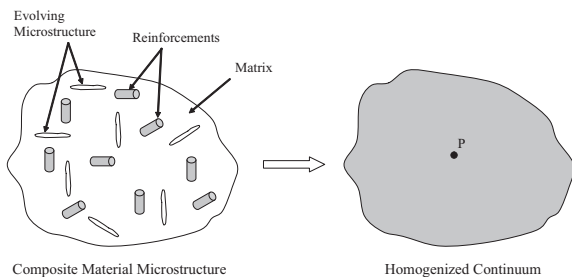


Fig. 2. Representation of a generic composite material with evolving microstructure (i.e., damage), and an effective homogenized continuum.

$$D_{ij}^{(\alpha)} = \frac{\kappa_\alpha t_\alpha^2}{s_\alpha t} n_i n_j \quad (2)$$

In this derivation, it is assumed that cracks in a single ply (i.e., one damage mode α) are evenly spaced, have the same surface area, and all run across the entire width of the RVE. The parameter t_α is the cracked ply thickness, s_α is the crack spacing, and $n_i = (\sin \theta, \cos \theta, 0)$ are crack surface normal unit vector components. The constraint parameter, κ_α , accounts for the constraining effect on ply cracks caused by adjacent plies in the laminate. Note that ply crack spacing is $s_\alpha = 1/\rho_\alpha$, where ρ_α is the corresponding crack density.

2.2. Constitutive law for homogenized laminate

To represent the damaged laminate as an effective linear elastic continuum, a typical Helmholtz free energy definition yields the following constitutive law, Singh and Talreja (2009):

$$\sigma_{ij} = C_{ijkl} (D_{ij}^{(\alpha)}) \varepsilon_{kl} \quad (3)$$

where σ_{ij} is the Cauchy stress tensor, ε_{ij} the strain tensor, and C_{ijkl} the stiffness tensor. Most laminates used in practice are thin, symmetric and balanced about their mid-plane, thus the formulation presented here will assume orthotropic material symmetry under plane stress. The general form of the stiffness tensor, utilizing Voigt notation, is given by:

$$C_{pq} = C_{pq}^0 - \sum_{\alpha} C_{pq}^{(\alpha)} \quad (4)$$

where C_{pq}^0 is the stiffness tensor for the undamaged material, and the $C_{pq}^{(\alpha)}$ terms correspond to changes in the stiffness tensor caused by the corresponding damage mode, α , which are functions of the damage tensor terms, $D_{ij}^{(\alpha)}$. The total stiffness tensor presented in Eq. (4) can be defined for a particular laminate consisting of any number of damage modes, α . In this study, four main classes of laminates will be studied: $[\mp\theta]_s$, $[0/90]_s$, $[0/\mp\theta/90]_s$, and $[0/90/\mp\theta]_s$.

A general laminate shown in Fig. 1 subjected to a multi-axial strain state may exhibit four distinct damage modes as indicated in Table 1. The $C_{pq}^{(\alpha)}$ terms for the first three damage modes are defined as, Singh and Talreja (2009):

Table 1

Damage modes considered in the SDM model.

Damage mode, α	Description
1	Matrix cracks in $-\theta$ plies
2	Matrix cracks in $+\theta$ plies
3	Matrix cracks in 90° plies
4	Matrix cracks in 0° plies

$$C_{pq}^{(1)} + C_{pq}^{(2)} = \frac{\kappa_0 t_0^2}{s_0 t} \begin{bmatrix} 2a_1^{(1,2)} & a_4^{(1,2)} & 0 \\ a_4^{(1,2)} & 2a_2^{(1,2)} & 0 \\ 0 & 0 & 2a_3^{(1,2)} \end{bmatrix} = D_\theta [a_i^{(1,2)}] \quad (5)$$

$$C_{pq}^{(3)} = \frac{\kappa_{90} t_{90}^2}{s_{90} t} \begin{bmatrix} 2a_1^{(3)} & a_4^{(3)} & 0 \\ a_4^{(3)} & 2a_2^{(3)} & 0 \\ 0 & 0 & 2a_3^{(3)} \end{bmatrix} = D_{90} [a_i^{(3)}] \quad (6)$$

The damage mode corresponding to cracking in the on-axis plies (i.e., $\alpha = 4$) is also included here due to multiaxiality, where the corresponding $C_{pq}^{(\alpha)}$ term is:

$$C_{pq}^{(4)} = \frac{\kappa_0 t_0^2}{s_0 t} \begin{bmatrix} 2a_1^{(4)} & a_4^{(4)} & 0 \\ a_4^{(4)} & 2a_2^{(4)} & 0 \\ 0 & 0 & 2a_3^{(4)} \end{bmatrix} = D_0 [a_i^{(4)}] \quad (7)$$

The $[a_i^{(\alpha)}]$ matrices contain material constants that correspond to each damage mode, α . The constraint parameters κ_θ , κ_{90} and κ_0 , the cracked ply thicknesses t_θ , t_{90} and t_0 , and the crack spacing terms s_θ , s_{90} and s_0 correspond to the $\pm\theta$, 90° and 0° plies, respectively. Note the cracked ply thicknesses appearing in Eqs. (5)–(7) depend on whether the cracked ply is centrally located or located away from the laminate mid-plane. For example, for the $[0/90]_s$ cross-ply laminate the cracked ply thicknesses are $t_0 = t_{ply}$, and $t_{90} = 2t_{ply}$, where t_{ply} is the thickness of a single ply.

It seems that since each damage mode has an independent $C_{pq}^{(\alpha)}$ term, there is no explicit coupling between the damage modes in the SDM model formulation. However, the constraint parameters, κ , are in fact the coupling terms, which will be detailed shortly. Using the expressions in Eqs. (5)–(7), the total stiffness for a specific laminate can be defined as follows:

$$C_{pq} = \begin{bmatrix} \frac{E_x^o}{1-\nu_{xy}^o \nu_{yx}^o} & \frac{\nu_{xy}^o E_y^o}{1-\nu_{xy}^o \nu_{yx}^o} & 0 \\ \frac{\nu_{xy}^o E_y^o}{1-\nu_{xy}^o \nu_{yx}^o} & \frac{E_y^o}{1-\nu_{xy}^o \nu_{yx}^o} & 0 \\ 0 & 0 & G_{xy}^o \end{bmatrix} - \sum_{\alpha} a_z D_z \begin{bmatrix} 2a_1^{(\alpha)} & a_4^{(\alpha)} & 0 \\ a_4^{(\alpha)} & 2a_2^{(\alpha)} & 0 \\ 0 & 0 & 2a_3^{(\alpha)} \end{bmatrix} \quad (8)$$

where E_x^o , E_y^o , G_{xy}^o , ν_{xy}^o , ν_{yx}^o are the longitudinal modulus, transverse modulus, in-plane shear modulus, and major and minor Poisson’s ratios, respectively, for the virgin laminate. The a_z terms are scalar integers that characterize the influence of crack size for a specific laminate given a particular stacking sequence, which account for the number

of plies in a given orientation. As an example, for a $[0/\mp\theta/90]_s$ laminate the total damage tensor is given by:

$$\begin{aligned} \sum_{\alpha} C_{pq}^{(\alpha)} &= 2\{C_{pq}^{(1)} + C_{pq}^{(2)}\} + C_{pq}^{(3)} + 2C_{pq}^{(4)} \\ &= 2D_\theta [a_i^{(1,2)}] + D_{90} [a_i^{(3)}] + 2D_0 [a_i^{(4)}] \end{aligned} \quad (9a)$$

Similarly for $[\mp\theta]_s$, $[0/90]_s$, and $[0/90/\mp\theta]_s$ laminates:

$$\sum_{\alpha} C_{pq}^{(\alpha)} = \{C_{pq}^{(1)} + C_{pq}^{(2)}\} = D_\theta [a_i^{(1,2)}] \quad (9b)$$

$$\sum_{\alpha} C_{pq}^{(\alpha)} = C_{pq}^{(3)} + 2C_{pq}^{(4)} = D_{90} [a_i^{(3)}] + 2D_0 [a_i^{(4)}] \quad (9c)$$

$$\begin{aligned} \sum_{\alpha} C_{pq}^{(\alpha)} &= \{C_{pq}^{(1)} + C_{pq}^{(2)}\} + 2C_{pq}^{(3)} + 2C_{pq}^{(4)} \\ &= D_\theta [a_i^{(1,2)}] + 2D_{90} [a_i^{(3)}] + 2D_0 [a_i^{(4)}] \end{aligned} \quad (9d)$$

The expression in Eq. (8) can be used to define the total stiffness tensor for any general symmetric laminate subjected to in-plane multiaxial loading, containing any number of damage modes and considered to have material orthotropic symmetry, so long as the constraint parameters, κ , and the material constants $a_i^{(\alpha)}$ for all relevant damage modes can be determined. In order to define the constraint parameters for a specific damage mode, the corresponding crack opening displacement (COD) is used and defined as the normal separation between the crack faces (i.e., direction 2 in Fig. 1). Thus, κ_α is defined by:

$$\kappa_\alpha = \frac{(\overline{\Delta u_2})_{(\alpha)}}{\varepsilon_{eff} t_z} \quad (10)$$

where $(\overline{\Delta u_2})_{(\alpha)}$ is the computationally evaluated COD averaged over the thickness of the ply. The average COD is normalized by the cracked ply thickness and effective strain, ε_{eff} , which is in fact the transformed strain component acting normal to the crack surface (i.e., $\varepsilon_{eff} = \varepsilon_{22}$). Transformed strain components are used here to incorporate multiaxial effects in the SDM model; this was not considered in previous models where only uniaxial loading was considered.

The material constant matrices (i.e., $[a_i^{(\alpha)}]$) depend on the active damage mode, and are left independent in Eq. (8) for multiaxial loading. This ensures that these terms are in fact constants, with a set of distinct values for each damage mode as shown in Eqs. (5)–(7). This also ensures that the influence of each damage mode on the evolving material engineering moduli (E_x , E_y , G_{xy} , ν_{xy} , ν_{yx}) are accurately captured. In previous work from Singh and Talreja (2009), these matrices were combined into one simple matrix with the assumption that they were constants with respect to off-axis ply orientation. The multiaxiality of the problem in the current study shows that this is in fact not applicable here. It should be noted that this linear damage formulation presented in Eq. (8) results in nonlinear stiffness predictions (see Section 4).

From the analytical stiffness-damage relationship defined in Eq. (8), the material engineering moduli for a damaged laminate can now be defined by the following relationships:

$$E_x = \frac{C_{11}C_{22} - C_{12}^2}{C_{22}}; \quad E_y = \frac{C_{11}C_{22} - C_{12}^2}{C_{11}}; \quad (11)$$

$$\nu_{xy} = \frac{C_{12}}{C_{22}}; \quad G_{xy} = C_{66}; \quad \nu_{yx} = \nu_{xy} \frac{E_y}{E_x}$$

Furthermore, in previous work the degradation of the damaged laminate in-plane shear modulus, G_{xy} , was not considered. In this study the in-plane shear modulus is considered due to the proper boundary conditions employed by the micromechanical simulation models (see Section 3), which is imperative since due to the multiaxial nature of the problem.

2.3. Nonlinear damage formulation

In the derivation of the constitutive relations presented in Section 2.2, it was assumed that only the first-order terms of the damage tensor components are considered in the definition of the Helmholtz free energy function. The model was recently expanded by Singh (2013) where the second-order terms of the damage tensor components were also considered in order to increase the model accuracy. The model developed here for multiaxial cases can similarly be expanded to include second-order damage terms, where the $C_{pq}^{(\alpha)}$ terms will have the following form:

$$C_{pq}^{(1)} + C_{pq}^{(2)} = D_\theta [a_i^{(1,2)}] + D_\theta^2 [b_i^{(1,2)}] \quad (12)$$

$$C_{pq}^{(3)} = D_{90} [a_i^{(3)}] + D_{90}^2 [b_i^{(3)}] \quad (13)$$

$$C_{pq}^{(4)} = D_0 [a_i^{(4)}] + D_0^2 [b_i^{(4)}] \quad (14)$$

The $[b_i^{(\alpha)}]$ matrices contain additional material constants that correspond to a specific damage mode, α . The total stiffness is therefore defined by:

$$C_{pq} = C_{pq}^0 - \sum_{\alpha} a_x D_{\alpha} \begin{bmatrix} 2a_1^{(\alpha)} & a_4^{(\alpha)} & 0 \\ a_4^{(\alpha)} & 2a_2^{(\alpha)} & 0 \\ 0 & 0 & 2a_3^{(\alpha)} \end{bmatrix} - \sum_{\alpha} a_x D_{\alpha}^2 \begin{bmatrix} 2b_1^{(\alpha)} & b_4^{(\alpha)} & 0 \\ b_4^{(\alpha)} & 2b_2^{(\alpha)} & 0 \\ 0 & 0 & 2b_3^{(\alpha)} \end{bmatrix} \quad (15)$$

3. Development of RVE for multiaxial stress states in multidirectional laminates

The main advantage of the SDM modeling approach is that it relies on computational micromechanics in lieu of experimental testing to calibrate the material damage parameters. In this study, computational micromechanics is employed to define the averaged CODs, $(\overline{\Delta u_2})_{(x)}$, as well as the material constant tensors, $[a_i^{(\alpha)}]$ and $[b_i^{(\alpha)}]$, corresponding to each damage mode for a specific laminate. The aim is to capture the constraining effects of the adjacent plies on a cracked ply of interest using 3D finite element (FE) analysis. This section describes new multiaxial capabilities that are added to the computational microme-

chanical FE model in order to define the crack surface displacements. Periodic boundary conditions (PBC) are properly applied to the FE model through the use of constraint equations as will be described here.

3.1. Repeating unit cell geometry and finite element model

For each laminate configuration considered, micromechanical FE models containing sub-critical ply cracks are generated in order to conduct the corresponding computational simulations. An appropriate RVE for the particular crack-containing laminate under consideration must be defined, which accurately represents the material properties, the ply specific geometry, and the orientation of the cracks present for a given damage state. Furthermore, if PBCs are invoked then the RVE must also be a repeating unit cell (RUC). It can be difficult to identify the repeating geometry for a laminate containing ply cracks in multiple orientations, although with some reasonable assumptions a RUC can always be defined.

For demonstration purposes, a $[0/90/\mp\theta]_s$ laminate containing ply cracks in multiple orientations will be considered because of its complexity. Due to symmetry about the mid-plane, a 3D RVE for the half-laminate containing cracks in each ply is used as shown in Fig. 3(a), where the cracked ply thickness for the 0° ply, the laminate half-thickness, and the RVE width are shown. The cracks in each ply are assumed to have uniform spacing as shown in Fig. 3(b), and are assumed to run across the entire width of the RVE. Since the RVE represents a small point in the continuum of the laminate as shown in Fig. 2, the latter assumption seems quite reasonable. The former assumption has been shown to be invalid when the crack spacing is quite high, but tends to be accurate as the crack spacing becomes smaller (Li et al., 2009). The cracks are also assumed to span through the thickness of the corresponding plies, which is consistent with experimental observations of unidirectional laminates. Furthermore, the cracks in each ply are also assumed to intersect at a single (x,y) location, which implies a state of maximum crack interaction. This may be considered a worst-case scenario, which may be slightly conservative at low crack densities (or high crack spacing). However, as the crack density increases the accuracy of this assumption also increases since cracks in different plies are most likely to interact. Experimental evidence by Tong et al. (1997) does suggest that cracks in different oriented plies begin at their common interfaces. This is due to the fact that the high stresses at the crack tips in one ply may cause a crack to initiate at that same location in an adjacent ply with a different orientation. Therefore, this is deemed the best choice for the micromechanical simulations.

Generally for the definition of the RVE, the crack spacing in plies of different orientations can be independent from one another. However, in order to specifically define a RUC, it is necessary to restrict the crack spacing of plies that have different orientations. For example, it must be ensured that the 90° ply crack spacing, s_{90} , is equal to or a multiple of the θ ply crack spacing projection on the x -direction, $s_{\theta x}$, as shown in Fig. 3(b). Similarly, the 0° ply crack spacing, s_0 , must be equal to or a multiple of the θ

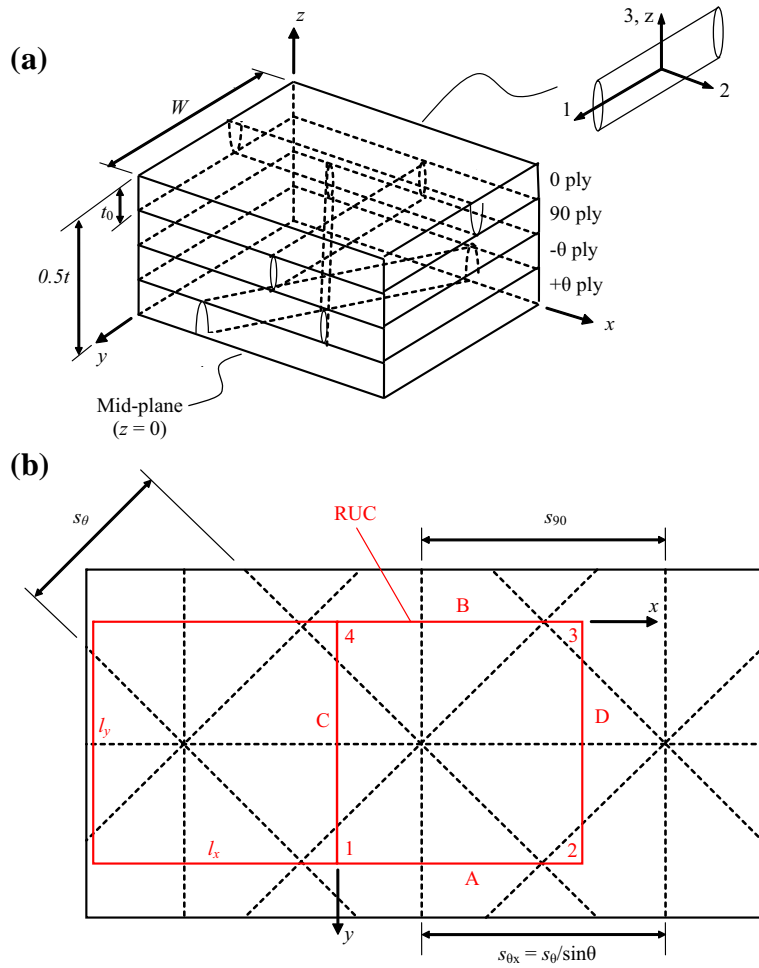


Fig. 3. A multidirectional $[0/90/\mp\theta]_s$ laminate containing ply cracks of multiple orientations (a) 3D geometry of RVE, (b) planar view of multidirectional cracks in the RVE, with the RUC indicated.

ply crack spacing projection on the y -direction, $s_{\theta y}$. These restrictions ensure that regardless of the number of damage modes present, a RUC can always be defined and proper periodic boundary conditions can be invoked. These restrictions have no bearing on the accuracy of the micro-mechanical FE models, and do not limit the model capabilities. Moreover, in order to simplify the equations that represent the PBC (see Section 3.2) it is also ensured that there are no crack surfaces on faces A, B, C and D of the RUC, and no crack tips on edges 1, 2, 3 and 4 of the RUC (see Fig. 3(b), where the RUC is offset slightly). This ensures that all cracks are internal to the RUC and that there are no issues applying the PBC, with the trade-off of a higher demand for meshing the RUC. It should be further noted that the size of the RVE in the x - y plane (see Fig. 3(b)) varies with the ply crack density (spacing), and that an RVE containing only one crack in each cracked ply is suitable for representing the mechanical properties of the laminate since PBCs are employed in this study.

With the RUC for a crack containing laminate defined, its geometry can be created within a suitable FE software package such as ANSYS. A number of three-dimensional

FE models are created for each laminate, for various crack densities and damage states using an automated process within the ANSYS APDL environment. For demonstration purposes, a $[0/90/\mp\theta]_s$ laminate containing ply cracks in multiple orientations will once again be considered. Each ply is modeled using 20-node SOLID186 brick elements; recall that a three-dimensional analysis is required to capture the constraining effects between adjacent plies and the out-of-plane deformation behavior. The element mesh is refined and the aspect ratio of the elements is maintained close to 1 in order to ensure a higher degree of accuracy. Mapped meshing is utilized in order to obtain a smooth flow of elements through the thickness of each ply. An example of a meshed RUC for a $[0/90/\mp45]_s$ half-laminate is shown in Fig. 4. Note that a mesh sensitivity analysis was performed and the 40,000 element mesh shown provides a good balance between result accuracy and solution time – improved mesh density has no bearing on the simulation results. The planar crack pattern shown in Fig. 3(b) was projected through each ply in the FE model in order to allow for a mesh with proper element-to-element connectivity. The nodes on the crack surface pairs

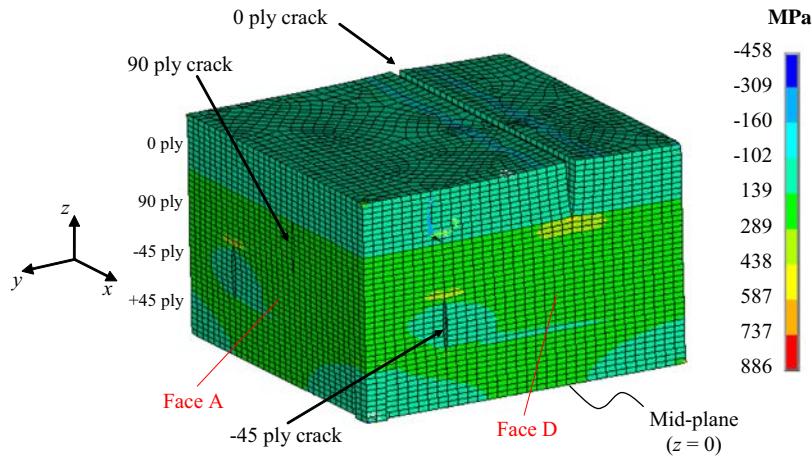


Fig. 4. FE mesh of a RUC for a $[0/90/\pm 45]_s$ laminate containing cracks in the 90° , 0° and $\pm 45^\circ$ plies. The RUC is loaded in biaxial tension along the x - and y -directions, where the stress contour for the stress component in the y -direction, σ_{yy} , is shown.

are not connected within the corresponding plies, which allows for proper displacement of the crack surfaces. However, the nodes on the interfaces between each ply are coinciding, which ensures continuity between the plies (i.e., no delamination).

The ply material considered in this study is a unidirectional glass fiber/epoxy (E-glass, Epikote 828/NMA/BDMA epoxy) system, with in-plane properties $E_1 = 46$ GPa, $E_2 = 13$ GPa, $G_{12} = 5$ GPa, $\nu_{12} = 0.3$. Each unidirectional ply is treated as a linear elastic transversely orthotropic material, thus the remaining properties for the 3D ply elements are: $E_3 = E_2 = 13$ GPa, $G_{13} = G_{12} = 5$ GPa, $\nu_{13} = \nu_{12} = 0.3$, and $G_{23} = 0.5E_2/(1 + \nu_{23}) = 4.64$ GPa, where the Poisson's ratio in the isotropic cross-sectional plane is taken as $\nu_{23} = 0.4$. The ply thickness for all laminates considered in this study is 0.5 mm. Note that plies are taken as homogenized materials with the presented material properties, thus the fibers and matrix are not explicitly modeled.

For thin laminates subjected to in-plane multiaxial strains, in-plane periodic boundary conditions are applied on the RUC in order to properly represent the local shear response. Symmetric boundary conditions are not applicable in this case, and are only suitable for uniaxial loading (Singh and Talreja, 2009). Furthermore, the applied PBC must ensure that the RUC considered here has proper displacement and traction boundary conditions in order to have continuity on its surfaces. Consider the RUC shown in Figs. 3 and 4 for a $[0/90/\mp\theta]_s$ laminate containing ply cracks. For the in-plane response PBCs must be applied between the nodes on opposing faces of the RUC due to multiaxial loading, mainly between face pair A and B and between face pair C and D. This involves imposing displacement constraints between these node pairs, and is accomplished in ANSYS by defining appropriate constraint equations as discussed by Lomov et al. (2007). For more details regarding the constraint equations and their relation to the applied strains, as well as specific meshing considerations, the reader is referred to Li et al. (2009). Furthermore, since only half of the laminate is considered due to symmetry, a symmetric boundary condition is added to the face of the RUC that corresponds to the lam-

inate mid-plane. The process of applying the periodic boundary conditions, as well as the additional constraints, to the FE model of the RUC are automated using ANSYS APDL programmable features.

3.2. COD and material damage constants

As indicated, the primary objectives for developing micromechanical FE models are to define the averaged CODs, $(\overline{\Delta u_2})_{(x)}$, as well as the material constant tensors, $[a_i^{(x)}]$ and $[b_i^{(x)}]$, corresponding to each damage mode for a specific laminate. Although the micromechanical FE models can also be used to define the crack sliding displacements (CSD), they are not currently utilized by the SDM model and therefore their consideration are left for a future study. The CSD corresponds to the relative displacement between the crack faces along direction 1 in Fig. 1, which is analogous to Mode II crack displacement. In order to define the averaged COD from the FE models, the relative displacement of the nodes on the corresponding crack surfaces must be considered. The CODs for a particular ply crack are averaged along the thickness of the ply, i.e., along the crack height, which corresponds to the z -direction in Fig. 3(a). Thus, the averaged COD is for damage mode α is defined as:

$$(\overline{\Delta u_2})_{(x)} = \frac{1}{t_x} \int_{-t_x/2}^{t_x/2} \Delta u_2(z) dz \quad (16)$$

where Δu_2 represents the separation of the crack surfaces in the 2-direction. Numerically, Eq. (16) is applied to the nodes on the corresponding crack surfaces through an automated post-processing algorithm developed using ANSYS APDL, which is invoked for a specific laminate.

Furthermore, for each laminate considered a number of micromechanical FE models are developed with various crack scenarios and cracks densities, which are analyzed under various multiaxial strain conditions. The goal here is to generate a database of COD data for each laminate, or generally for each class of laminates, in order to allow

for stiffness predictions and eventually damage evolution predictions of multidirectional laminates. Again, due to the availability of ANSYS APDL programmable features, an algorithm is easily created to automate this process, and therefore generate a large enough database for each laminate. In order to correlate the data for each laminate considered, the CODs are normalized by an effective strain value, ϵ_{eff} , and the cracked ply thickness, t_x . Therefore, the normalized COD is defined by:

$$(\widetilde{\Delta u_2})_{(x)} = \frac{(\Delta u_2)_{(x)}}{\epsilon_{eff} t_x} \quad (17)$$

The effective strain is again the transformed strain component in the local lamina level coordinate system acting normal to the corresponding crack surface, ϵ_{22} . This is the strain component directly acting on the crack surfaces, thus this strain transformation allows the model to consider the multiaxiality of the problem. The form of $(\widetilde{\Delta u_2})_{(x)}$ is in fact analogous to the constraint parameter defined by Eq. (10). It should be noted that $(\widetilde{\Delta u_2})_{(x)}$ depends only on the crack densities of the cracked ply and in the constraining plies, but not on the applied strain state or the cracked ply thickness. Therefore this is a convenient way to capture the crack displacements, and provides a means to easily correlate the data.

In order to evaluate the material constants for the different damage modes of a specific laminate, $a_i^{(\alpha)}$, the elasticity tensor for the undamaged laminate, C_{pq}^0 , is defined using CLT and the elasticity tensor for the damaged laminate, C_{pq} , is evaluated from a series of micromechanical FE simulations. In order to evaluate C_{pq} , a micromechanical FE model is created with one damage mode present having an arbitrary crack density, where the corresponding D_x term is evaluated using the corresponding expression from Eq. (5)–(7). Three simulations are conducted using the micromechanical FE model with different applied strains: (i) ϵ_{xx} , (ii) ϵ_{yy} , and (iii) γ_{xy} . For each simulation the volume averaged stresses and strains from the RUC are calculated using Eqs. (18a) and (18b), by considering the individual element stresses, σ_{ij} , and strains, ϵ_{ij} , as well as the RUC total volume, V .

$$\overline{\sigma}_{ij} = \frac{1}{V} \int_V \sigma_{ij} dV = \frac{1}{V} \sum_n \sigma_{ij}^n V^n \quad (18a)$$

$$\overline{\epsilon}_{ij} = \frac{1}{V} \int_V \epsilon_{ij} dV = \frac{1}{V} \sum_n \epsilon_{ij}^n V^n \quad (18b)$$

The parameter n is the total number of elements in the RUC. The volume averaged stresses and strains are then used to evaluate C_{pq} using Eq. (3). The $a_i^{(\alpha)}$ terms corresponding to the relevant damage mode can then be evaluated using Eq. (8). This process is repeated for each damage mode for the particular laminate. Note that if the nonlinear damage model defined by Eq. (15) is invoked, additional material constants, $b_i^{(\alpha)}$, must also be defined as is detailed in Singh (2013).

4. Results and discussion

A schematic of the overall synergistic multiscale modeling approach is shown in Fig. 5, which highlights the computational micromechanics component, as well as the continuum and structural modeling scales. In this Section, the computational micromechanical models will be validated and used to calibrate the SDM model before it is employed for predicting stiffness degradation of damaged laminates.

4.1. Validation of micromechanical FE model

In order to gain confidence in the developed laminate FE models, their accuracy will be verified with regards to the imposed periodic boundary conditions for representing multiaxial loading states and shear deformational response, and predictions for stiffness property reduction with increasing crack densities. Consider the same FE model shown in Fig. 4 for a $[0/90/\mp 45]_s$ laminate with cracks in each of the 0° , 90° and 45° plies, loaded with a shear strain of $\gamma_{xy} = 1\%$. The planar view of the RUC model shown in Fig. 6 depicts the required displacement continuity between these same face pairs. This can further be confirmed from the plot of the 2×2 array of the deformed

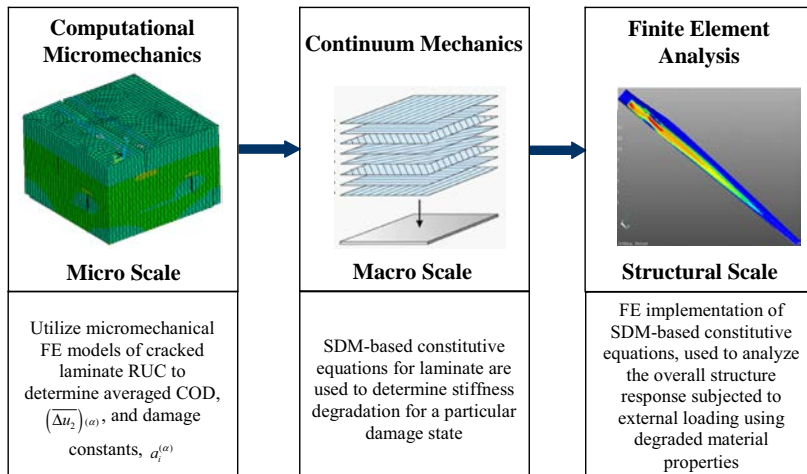


Fig. 5. Schematic of multiscale synergistic damage mechanics model.

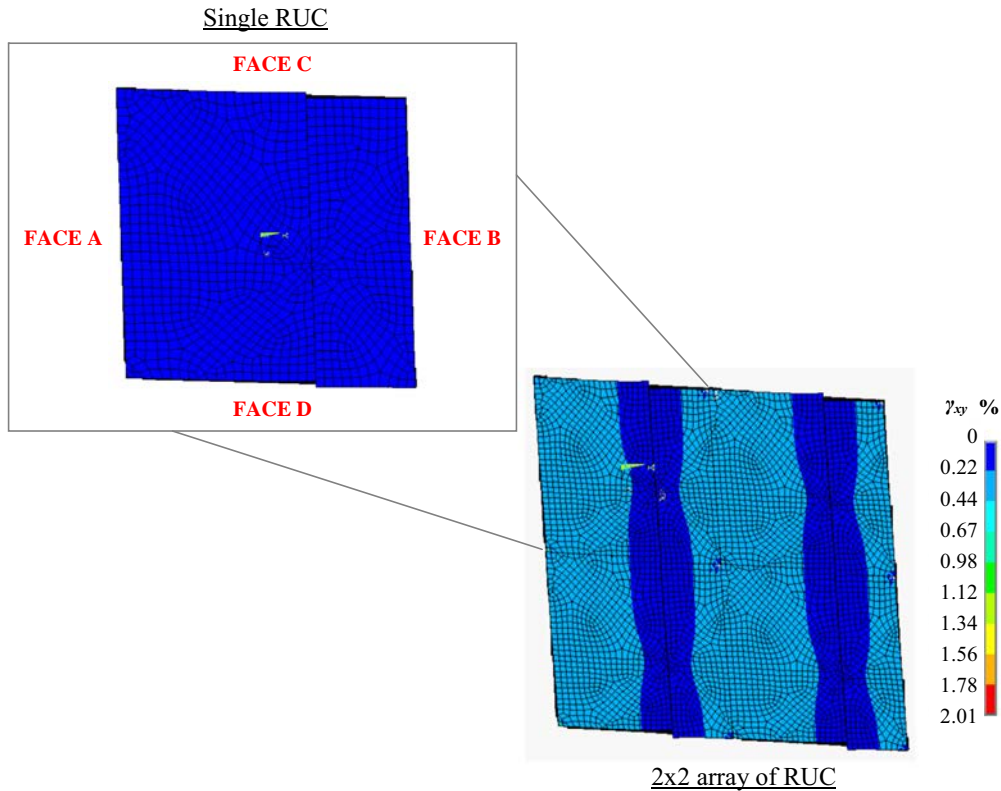


Fig. 6. Planar view of deformed RUC and a 2×2 array of the deformed periodic RUC for the $[0/90/\pm 45]_s$ laminate.

periodic RUCs also shown in Fig. 6, for which the adjacent boundaries are shown to be perfectly mated. The shear strain contours shown in the 2×2 array also reveal the continuity across the boundaries of the RUCs, which also highlights the ability of the developed FE models to accurately capture the laminate shear response. Although not presented, the required traction continuity conditions on the RUC boundaries are also satisfied.

Next, the RUC models are tested for their accuracy in predicting the undamaged laminate homogenized material properties. RUCs without any cracks are generated for three of the laminates considered, mainly $[\pm 45]_s$, $[0/90]_s$, and $[0/90/\pm 45]_s$ laminates. For each RUC, three simulations are conducted with different applied strains: (i) ε_{xx} , (ii) ε_{yy} , and (iii) γ_{xy} , where for each simulation the volume averaged stresses and strains are calculated using Eqs. (18a) and (18b). The laminate engineering constants are then evaluated from Eq. (11). In order to provide a basis for comparison, CLT was also used to determine the undamaged laminate properties. The computationally predicted undamaged laminate properties were within 0.5% of the theoretical values, providing confidence in the applied PBCs and the quality of the generated FE mesh.

Finally, using a similar procedure described in the previous paragraph, the accuracy of the micromechanical FE models in directly predicting stiffness properties of the damaged laminates will be verified against available experimental data for $[0/90]_s$ and $[0/90/\pm 45]_s$ glass fiber/

epoxy laminates subjected to uniaxial tensile loading (Tong et al., 1997). Since the crack densities were reported in the literature, the micromechanical FE models are tested at these same crack densities in order to provide a direct comparison. Plots of the normalized axial stiffness, E_x/E_x^0 , and in-plane Poisson's ratio, ν_{xy}/ν_{xy}^0 , as functions of the 90° ply crack density for both laminates are shown in Fig. 7. Clearly, the FE model predictions are in excellent agreement with the experimental results for both cases. These micromechanical FE models will be used later to compare the accuracy of the analytical SDM model predictions for multiaxial conditions.

4.2. Multiaxial effects on crack opening displacements

The micromechanical FE models will now be used to calibrate the SDM model for each laminate considered. As indicated in Section 3, a database of COD data was generated for the $[\pm\theta]_s$, $[0/90]_s$, $[0/\mp\theta/90]_s$, and $[0/90/\mp\theta]_s$ laminate configurations. For each class of laminate configuration, various cracking scenarios involving multiple crack densities and several multiaxial strain conditions were analyzed. The loading cases considered here include uniaxial tension, biaxial tension, coupled tension and shear, with various strain magnitudes ranging from 0.25% to 1.00%. Fig. 8 shows the variation of 90° ply COD for a $[0/90/\pm 45]_s$ laminate over the cracked ply thickness for the indicated applied strain states. The same crack density

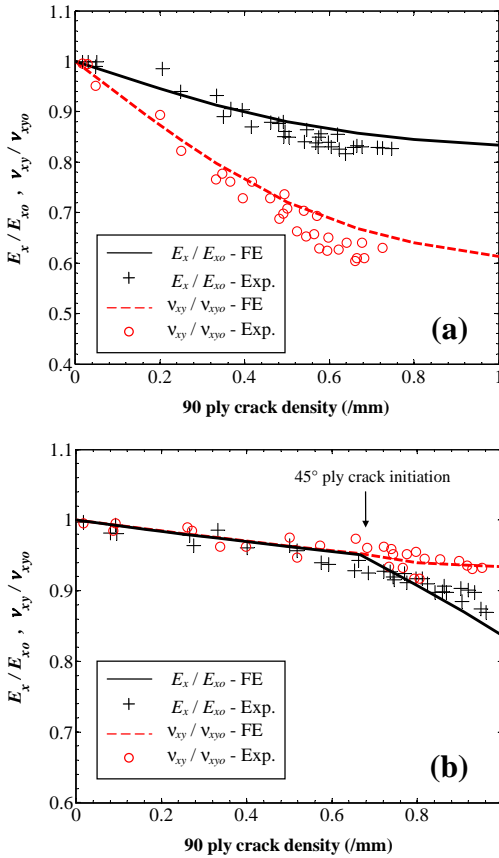


Fig. 7. Experimental and FE normalized axial stiffness and Poisson's ratio for (a) $[0/90]_s$ laminate, and (b) $[0/90/\pm 45]_s$ laminate. Uniaxial tensile experimental data was obtained from Tong et al. (1997).

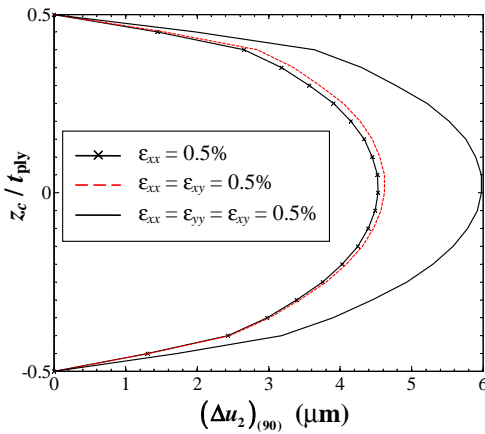


Fig. 8. $[0/90/\pm 45]_s$ laminate micromechanical FE prediction: variation of 90° ply crack surface nodal displacements (COD) over the 90° ply thickness.

was used for all plots, and only 90° ply cracks were included in the model. The COD has a maximum magnitude at the center of the ply (i.e., $z_c/t_{ply} = 0$), which is expected. It is clear that the addition of shear strain has a

negligible effect on the magnitude of the 90° ply COD. The addition of the tensile strain component ϵ_{yy} does however notably increase the COD as shown. This is due to the negative contraction of the laminate in the z -direction. Similar plots for CODs of 45° ply cracks are shown in Fig. 9 for the same $[0/90/\pm 45]_s$ laminate, for the case when both 90° ply and 45° ply cracks are present. Here, the addition of the tensile strain component ϵ_{yy} does increase the 45° ply COD, as is also the case for the 90° ply cracks. Note however that a further addition of shear strain causes the COD to decrease significantly, which is a result of a decreased strain component acting normal to the 45° ply crack surface (i.e., ϵ_{22}). It is also interesting to note that for a biaxial tensile strain scenario, the magnitude of the 45° ply COD is identical for different strain magnitudes (i.e., $\epsilon_{xx} = \epsilon_{yy} = 0.5\%$, and $\epsilon_{xx} = 0.75\%$, $\epsilon_{yy} = 0.25\%$), which is due to identical crack surface normal strain components. Although the results presented in Figs. 8 and 9 are intuitive, they are important for two reasons. First, they clearly highlight the effects of multiaxial strain states on crack surface displacement in multidirectional laminates, and demonstrate that the micromechanical FE models properly capture this behavior. The importance of the transformed strain components in the local lamina coordinate system for each particular damage model is also illustrated, as is their influence on the magnitudes of the CODs. Secondly, these results further confirm the accuracy of the developed FE models and the imposed PBCs.

Since the average CODs are proportional to the applied strain, they can be normalized as shown in Eq. (17) to provide a better way to correlate all the simulation data for each laminate. Nevertheless, it is noted that the magnitude of the normalized crack displacements depend upon: (i) crack density for the particular crack of interest, and (ii) crack density in the adjacent plies.

First, consider the $[0/90]_s$ cross-ply laminate containing ply cracks in the 90° plies only. A plot of the normalized 90° ply COD as a function of the 90° ply crack density is

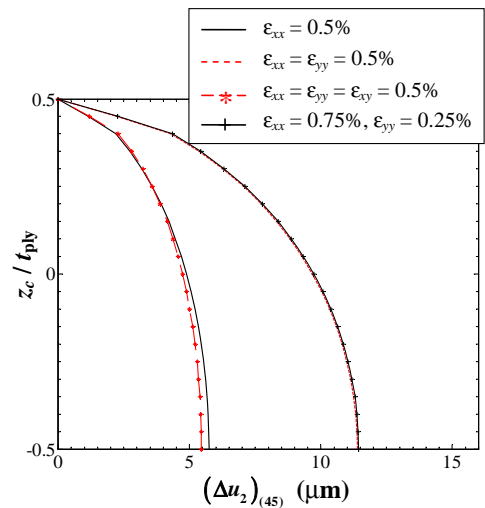


Fig. 9. $[0/90/\pm 45]_s$ laminate micromechanical FE prediction: variation of $+45^\circ$ ply crack surface nodal displacements (COD) over the $+45^\circ$ ply thickness.

shown in Fig. 10(a). The normalized COD decreases as the crack density increases due to the interactive shielding effect between the neighboring cracks in a given layer. An inverse sigmoidal function can be used to fit the normalized COD-crack density data:

$$(\widetilde{\Delta u}_2)_{(\alpha)} = \frac{c_1}{1 + c_2 \rho_x^{c_3}} \quad (19)$$

It can be seen from Fig. 10(a) that this function accurately captures the gradual decrease in $(\widetilde{\Delta u}_2)_{(\alpha)}$ for very low crack densities, while also capturing the steep decrease at intermediate to high crack densities. The corresponding fitting coefficients, c_1 , c_2 and c_3 , are listed in Table 2. It should be noted that for the $[0/90]_s$ laminate the inverse sigmoidal function coefficients are independent of the 0° ply crack density, which implies that the 0° plies do not alter the constraining effects on the normalized 90° ply CODs. This is not surprising since the deformation of the 0° ply in the direction normal to the 90° ply crack surfaces will not depend on the 0° ply crack density. For cross-ply laminates, this allows for the definition of a unique inverse sigmoidal function for each damage mode that is independent of the other damage modes. The normalized 0° ply CODs and the corresponding fitting function are plotted in Fig. 10(b), with the corresponding fitting coefficients listed in Table 2.

Now consider a $[0/90/\mp 45]_s$ laminate with cracking in the 0° , 90° and 45° plies. The normalized 0° ply COD obtained from the FE simulations are plotted in Fig. 11 along with the corresponding inverse sigmoidal fitting function. Although the 90° ply is adjacent to the 0° ply, the normalized 0° ply COD have no dependence on the 90° ply crack density due to the crack relative positions (i.e., perpendicular). Note that the 45° ply crack density has no bearing on the normalized 0° ply COD in this case since these plies are not adjacent within the laminate. Also note that this may not necessarily be the case if the 0° and 45° ply cracks were closer in proximity (i.e., if the 90° layer was very thin). The corresponding fitting function coefficients are listed in Table 3. Moreover, the normalized 90° ply COD are independent of the 0° ply cracks, but are influenced by the 45° ply crack density as shown in Fig. 12. This is due to the fact that any deformation in the 45° plies normal to the 90° ply crack surfaces will increase as the 45° ply crack density, and thus the ply compliance, increases. This decreases the constraining effect on the 90° plies and thus increases the normalized 90° ply COD as shown. The corresponding inverse sigmoidal fitting function

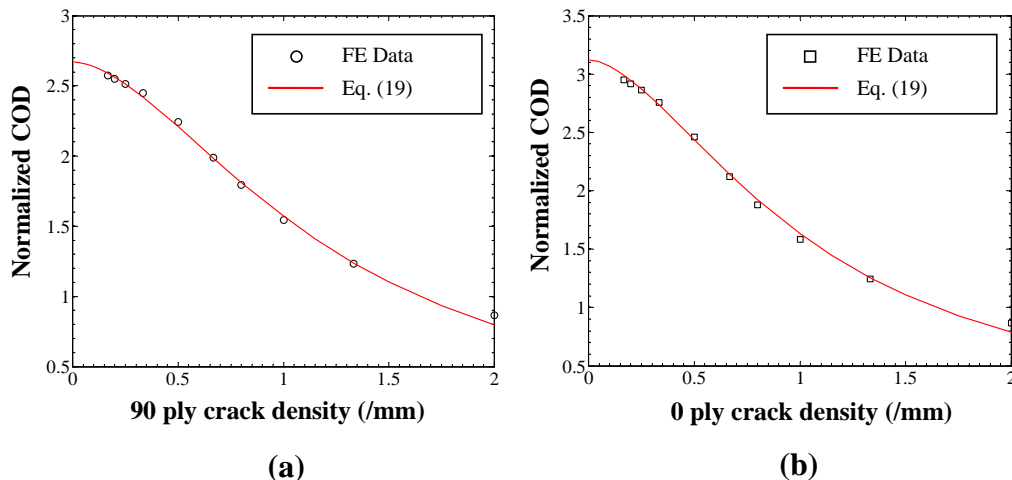


Fig. 10. $[0/90]_s$ laminate micromechanical FE prediction: (a) normalized 90° ply COD, and (b) normalized 0° ply COD plotted as functions of crack density. The data in both plots have also been fitted using the inverse sigmoidal function.

Table 2

Inverse sigmoidal fitting function coefficients from Eq. (19) for $[0/90]_s$ laminate.

Damage mode	c_1	c_2	c_3
90° ply COD	2.67	0.70	1.75
0° ply COD	3.12	0.91	1.70

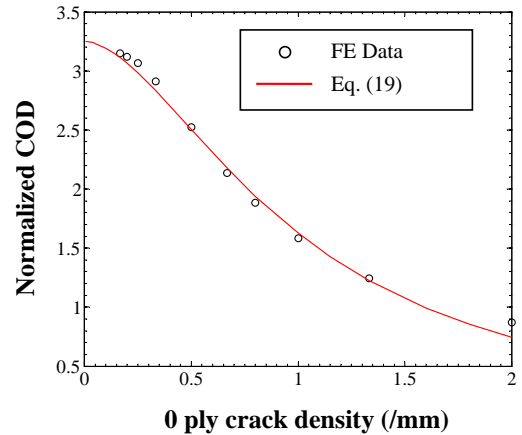


Fig. 11. $[0/90/\mp 45]_s$ laminate micromechanical FE prediction: normalized 0° ply COD plotted as a function of crack density. The data has been fitted using the inverse sigmoidal function.

Table 3
Inverse sigmoidal fitting function coefficients from Eq. (19) for [0/90/±45]_s laminate.

Damage mode	c ₁	c ₂	c ₃
90° ply COD	0.0263ρ ₄₅ + 1.2672	0.0192ρ ₄₅ + 0.2021	1.8
0° ply COD	3.25	1.00	1.75
+45° ply COD	2.57	0.62	1.77
−45° ply COD	1.27	0.16	2.10

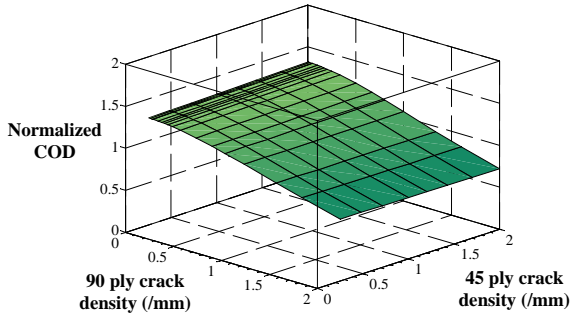


Fig. 12. [0/90/±45]_s laminate micromechanical FE prediction: normalized 90° ply COD 3D plot.

coefficients are listed in Table 3, which also includes the fitting function coefficients for the normalized 45° ply CODs. Crack displacements in the +45° plies are not influenced by the 0° and 90° ply cracks since these plies are not adjacent (i.e., the +45° plies are at the laminate mid-plane). Crack displacements in the −45° plies are slightly influenced by the 90° ply crack density, but this is found to be negligible.

4.3. SDM stiffness predictions

In order to highlight the predictive capabilities of the SDM model for multiaxial conditions, the stiffness degra-

Table 4
Laminate material properties (CLT).

Laminate	E _x ^o (GPa)	E _y ^o (GPa)	G _{xy} ^o (GPa)	ν _{xy} ^o
[±45] _s	15.48	15.48	13.14	0.548
[0/90] _s	30.25	30.25	5.00	0.13
[0/90/±45] _s	26.20	26.20	9.10	0.30

Table 5
Damage tensor material constants corresponding to the listed damage mode for each indicated laminate.

Damage mode	[0/90] _s			[0/90/±45] _s			[±45] _s		
	90°	0°	±45°	90°	0°	±45°	90°	0°	±45°
a ₁ ^(x) (GPa)	6.80	0.59	–	7.74	0.68	9.71	–	–	8.94
a ₂ ^(x) (GPa)	0.59	6.77	–	0.66	7.80	9.50	–	–	8.97
a ₃ ^(x) (GPa)	1.49	1.22	–	1.41	1.05	1.78	–	–	1.83
a ₄ ^(x) (GPa)	4.02	4.00	–	4.52	4.61	6.15	–	–	7.36
b ₁ ^(x) (GPa)	0.90	0.12	–	4.57	0.16	3.59	–	–	0.20
b ₂ ^(x) (GPa)	0.08	1.25	–	0.39	−3.41	4.19	–	–	−0.10
b ₃ ^(x) (GPa)	0.43	1.53	–	1.77	4.64	−0.60	–	–	−0.51
b ₄ ^(x) (GPa)	0.53	0.74	–	2.65	−0.47	0.47	–	–	−7.14

duction for the aforementioned laminates will be evaluated using Eqs. (8) and (15). As shown in Fig. 5, the data required includes: (i) the undamaged laminate properties defined in Table 4, (ii) the damage parameters which are computed from micromechanical FE simulations and are presented in Tables 2 and 3, (iii) the material damage constants a_i^(x) and b_i^(x). The corresponding material constants for each damage mode can be defined as outlined in Section 3.2, which are listed in Table 5 for each laminate considered here. It should be restated that due to the proper PBC invoked by the micromechanical FE models, it is possible to track the laminate shear behavior (G_{xy}), and thus define the material constants a₃ and b₃. This is a key contribution in the development of the SDM prediction model, which is vital for including multiaxiality in the SDM model. It is important to note that both CODs and damage constants can also be computed from experimental data whenever available, as was shown in previous studies (Varna et al., 1999; Singh and Talreja, 2009). Furthermore, it is noted here that while previous SDM models defined CODs to be independent of crack density, that assumption has been relaxed here so as to account for interactions between stress fields of neighboring cracks. Note for the predictions conducted here, only the COD is considered in the SDM model. Also for the laminates containing ±θ ply cracks, the constraint parameters for the +θ and −θ plies are averaged for the SDM predictions. This assumption has previously been found to provide adequate results since experimental evidence suggests that the crack densities in these plies tend to be quite similar (Singh and Talreja, 2009). Furthermore, since experimental data for multiaxial loading of laminates is currently lacking in the literature, the micromechanical FE models are also used to directly determine the laminate stiffness degradation. This will provide a way to evaluate the accuracy of the trends with the analytical SDM stiffness predictions for multiaxial cases. The FE models for each laminate considered here account for specific multiple damage scenarios with various cracks densities, thus they provide adequate independent prediction data for comparison. Note that experimental data would in fact be required in order to validate the prediction model. A similar procedure defined in Section 4.1 is followed for this purpose, however the laminate FE models will now contain the appropriate ply crack scenarios.

Various evolving multidirectional damage states that correspond to multiaxial loading conditions are analyzed for the analytical SDM model predictions. For a $[0/90]_s$ cross-ply laminate, two evolving damage states are considered as are listed in Table 6. The first damage state may result from uniaxial loading in the longitudinal direction, ε_{xx} , as it describes cracks in the 90° plies only, but may also occur from combined ε_{xx} and γ_{xy} loading. The second evolving damage state corresponds to a biaxial loading condition where $\varepsilon_{xx} = \varepsilon_{yy}$. Plots of the normalized engineering moduli for damage state 1 are shown in Fig. 13, which include the linear and nonlinear SDM model predictions, as well as the computational FE data. It is clear from the plots that the SDM predictions using the linear damage terms in the constitutive model (i.e., Eq. (8)) correlate well with the FE data. The nonlinear SDM predictions using Eq. (15) show a slight improvement when compared to the linear SDM predictions for the in-plane shear modulus. Since only 90° ply cracks are present, all engineering moduli, except for the transverse modulus, undergo notable degradation. Also, degradation of the in-plane shear modulus, G_{xy} , occurs at a faster rate when compared to degradation of the axial modulus, E_x , but at a slower rate than the major Poisson's ratio, ν_{xy} . Similar trends were also reported Kashtalyan and Soutis (2013) for similar glass/epoxy cross-ply laminates. Plots of the normalized engineering

moduli for damage state 2 are shown in Fig. 14. Once again, the SDM predictions correlate very well with the FE model data. Here, the axial and transverse moduli degrade with a similar rate since the evolution of the crack density in the 90° and 0° plies is assumed to be concurrent as is shown in Table 6. This is expected since the cross-ply laminate only contains two outer 0° plies and two inner 90° plies of the same thickness. Once again the Poisson's ratio shows the greatest degradation of all the engineering moduli. For damage state 2, both the Poisson ratio and the shear modulus exhibit greater degradation compared to damage state 1. This is due to the existence of the 0° ply cracks which enhances the degradation of these parameters as shown in Figs. 13 and 14. This reveals the combined effect of the two damage modes on the laminate properties, which also demonstrates the multiaxial capability of the SDM model.

In previous SDM models, the stiffness degradation plots were linear when linear damage terms were used in the constitutive equations (i.e., Eq. (3)). Fig. 13(a) also includes plots of the normalized axial stiffness and Poisson's ratio determined from the same linear model used by Singh and Talreja (2009). The main reason for this predicted linearity in the plots is that there was a single set of damage constants, $a_i^{(x)}$, for a particular laminate. In the present study, the segregation of the different damage modes in the constitutive equations allows for the definition of a different set of constants for each damage mode. This consequently allows the SDM model to capture the nonlinear stiffness degradation since the effects of each specific damage mode have manifested through the stiffness predictions. Furthermore, in previous studies the CODs and corresponding constraint parameters were assumed to be constant with increasing crack density, and thus the interaction between stress fields of neighboring cracks, which is appreciable at medium to high crack densities, was not accounted for. In this study, the model has been improved by accounting for the variation of CODs as damage evolves (see Eq. (19)). Nevertheless, this does increase the model complexity by requiring necessary FE computations. Overall, the outcome of these changes in the definition of the

Table 6
Evolving crack densities used for $[0/90]_s$ cross-ply laminate predictions.

Damage state 1		Damage state 2	
ρ_{90} (/mm)	ρ_0 (/mm)	ρ_{90} (/mm)	ρ_0 (/mm)
0	–	0	0
0.1667	–	0.1667	0.1667
0.2	–	0.2	0.2
0.25	–	0.25	0.25
0.333	–	0.333	0.333
0.5	–	0.5	0.5
0.6667	–	0.6667	0.6667
0.8	–	0.8	0.8
1.0	–	1.0	1.0

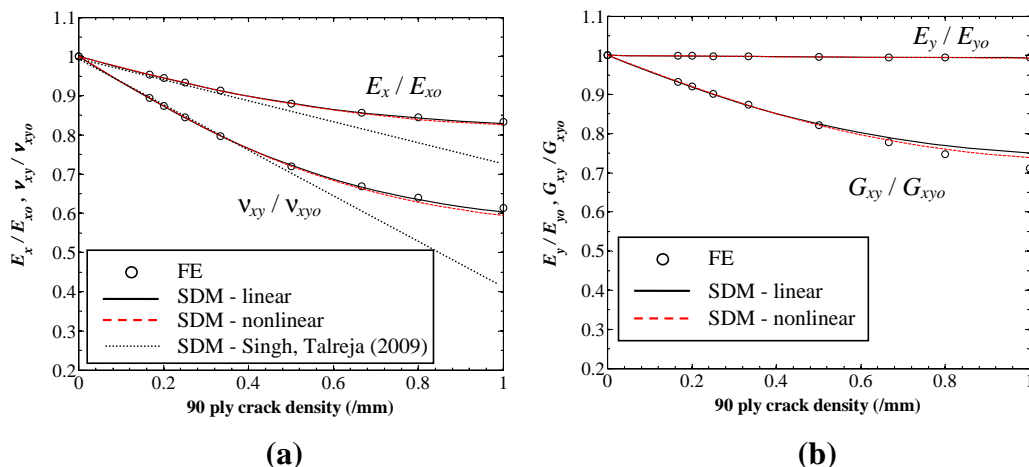


Fig. 13. $[0/90]_s$ laminate predicted normalized engineering moduli as functions of ρ_{90} for damage state 1 (see Table 6).

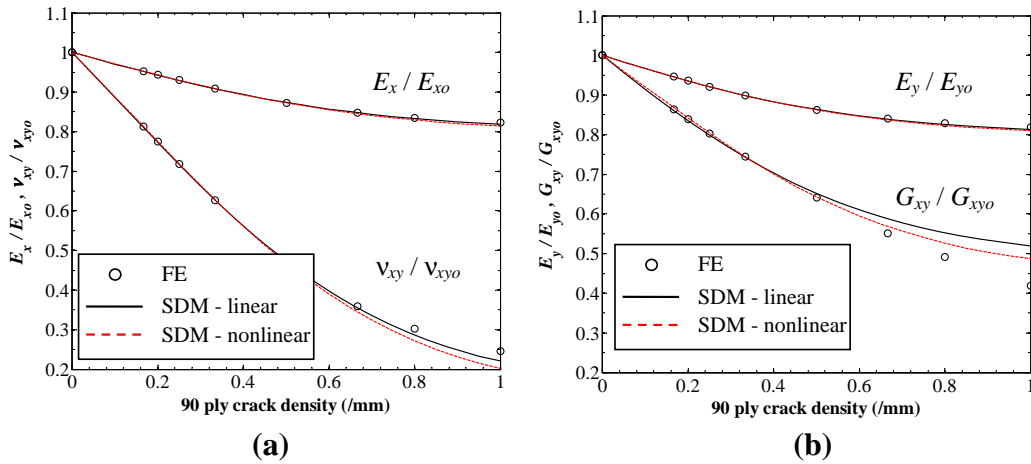


Fig. 14. [0/90]_s laminate predicted normalized engineering moduli as functions of ρ_{90} for damage state 2 (see Table 6).

constraint parameters and the overall stiffness tensor is that the nonlinearity in stiffness reductions can be captured even by the linear SDM model that considers first order damage modes (see Figs. 13 and 14). For simplicity, the predictions using the nonlinear SDM model will be shown hereafter.

For the [0/90/±45]_s quasi-isotropic laminate, the two damage states considered are listed in Table 7. The first damage state considered may result from either uniaxial loading, ϵ_{xx} , or from combined ϵ_{xx} and γ_{xy} loading. The second damage state corresponds to a biaxial loading condition where $\epsilon_{xx} = \epsilon_{yy}$. Plots of the normalized engineering moduli for both cases are shown in Figs. 15 and 16, respectively. Once again, the analytical SDM model predictions correlate very well with the FE data for both evolving damage states. Fig. 15(a) reveals that the degradation of the axial modulus for damage state 1 is initially very gradual and caused solely by the 90° ply cracks. Once the 45° ply cracks initiate the axial modulus degrades at an advanced rate, in agreement with experimental observations (Tong et al. (1997)) for a uniaxial loading case. A similar trend is found with the Poisson’s ratio and the in-plane shear modulus. Furthermore, the axial modulus degrades more than the transverse modulus due to the contributions of both 90° and 45° ply cracks. Since 90° ply cracks do not

contribute to reduction in transverse modulus, it only begins to degrade once the 45° ply cracks initiate, thus leading to a less severe degradation for damage state 1. For multiaxial damage state 2, the 45° ply cracks initiate sooner and 0° ply cracks evolve concurrently with the 90° ply cracks, therefore there is greater degradation for all engineering moduli as shown. The degradation of the axial and transverse moduli occurs at a similar rate in this case, which is due to the addition of the 0° ply cracks. The 0° ply cracks cause a similar increase in compliance in the transverse direction as the 90° ply cracks cause in the axial direction, which is expected since the laminate contains the same number of 90° and 0° plies. Note that since the 0° plies are outer plies and only constrained on one side, they have caused a slightly greater stiffness degradation in the transverse direction when compared to the effect of the inner 90° plies on the axial modulus. This reveals the combined effect of the two damage modes on the laminate properties, as well as the multiaxial capability of the prediction model.

Finally, for the [±45]_s angle-ply laminate only one evolving damage state is considered since there is only one effective damage mode. The evolving crack densities in the 45° plies are defined as 0, 0.23, 0.35, 0.47, 0.707, 0.94, 1.13 and 1.28 mm⁻¹, which can result from a uniaxial

Table 7
Evolving crack densities used for [0/90/±45]_s quasi-isotropic laminate predictions.

Damage state 1			Damage state 2		
ρ_{90} (/mm)	ρ_{45} (/mm)	ρ_0 (/mm)	ρ_{90} (/mm)	ρ_{45} (/mm)	ρ_0 (/mm)
0	0	-	0	0	0
0.1667	0	-	0.1667	0	0.1667
0.2	0	-	0.2	0	0.2
0.25	0	-	0.25	0	0.25
0.333	0	-	0.333	0.235	0.333
0.5	0	-	0.5	0.707	0.5
0.6667	0	-	0.6667	0.942	0.6667
0.8	0.226	-	0.8	1.13	0.8
0.9	0.643	-	0.9	2.57	0.9
1.0	0.707	-	1.0	2.82	1.0

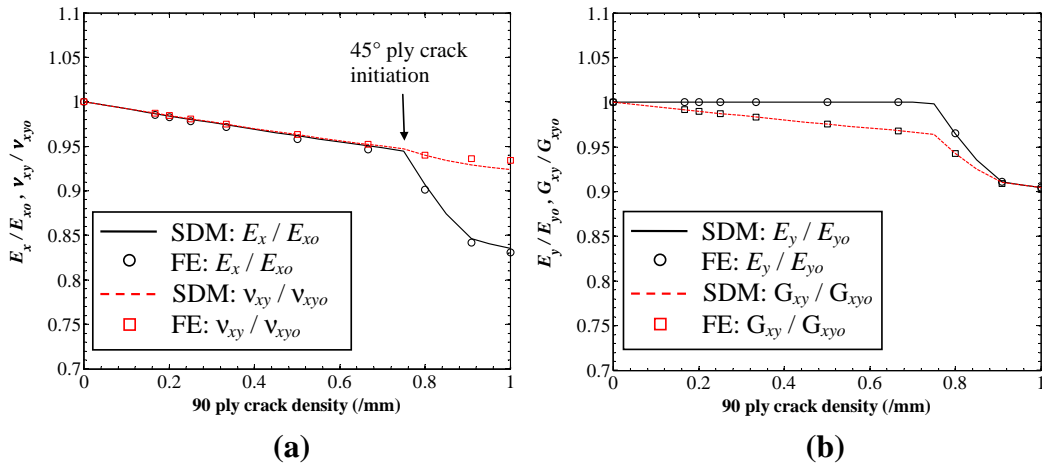


Fig. 15. $[0/90/\pm 45]_s$ laminate predicted normalized engineering moduli as functions of ρ_{90} for damage state 1 (see Table 7).

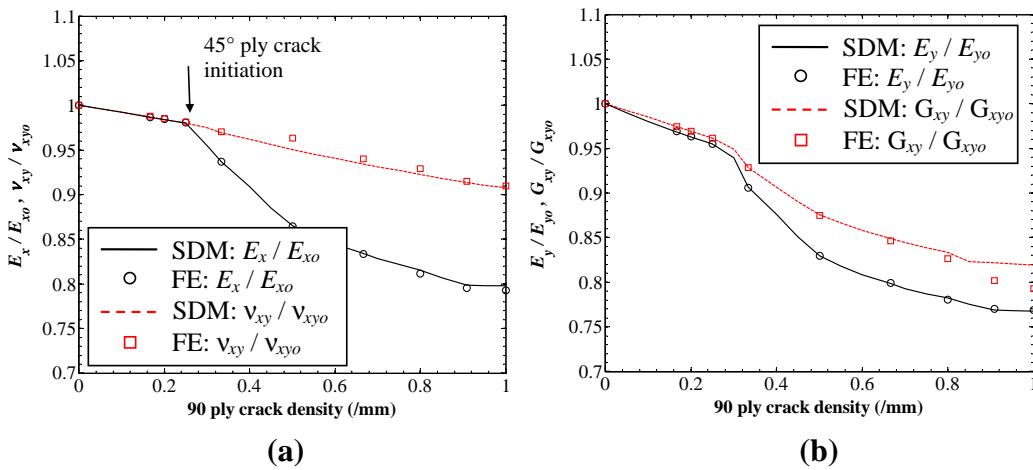


Fig. 16. $[0/90/\pm 45]_s$ laminate predicted normalized engineering moduli as functions of ρ_{90} for damage state 2 (see Table 7).

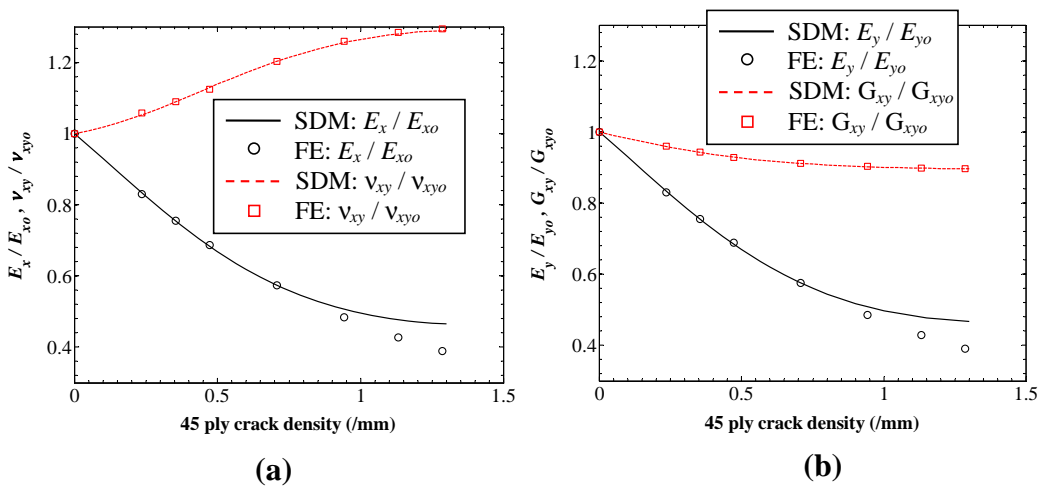


Fig. 17. $[\pm 45]_s$ laminate predicted normalized engineering moduli as functions of ρ_{45} .

strain condition or any multiaxial strain state. Plots of the corresponding normalized engineering moduli are shown in Fig. 17, and again the analytical SDM predictions correlate very well with the FE data. The degradation of both the axial and transverse moduli are significant since there are no other plies reinforcing the laminate. Also, the axial and transverse moduli degrade at the same rate which is expected for the angle-ply laminate. The increase of the Poisson's ratio by approximately 30% at 1.2 mm^{-1} crack density, as shown in Fig. 17a, may seem to be an unexpected result. However, a study by Varna (2008) has shown that for a similar $[0/\pm 45/0]_s$ laminate this was also the case, which was supported in the same study by experimental evidence. This is likely a result of shear modulus degradation and the fact that the axial and transverse moduli degraded with the same rate, leading to an increasing Poisson's ratio.

5. Model discussion

The SDM-based prediction model developed in this study involved a number of complex augmentations in order to include multiaxial effects. First, an additional damage mode (i.e., cracking in the on-axis plies, $\alpha = 4$) was included in the SDM model. This was necessary in order to account for additional damage scenarios that correspond to practical multiaxial strain states. As a result, the SDM model can now be used for any general symmetric laminate with plies containing cracks oriented in multiple directions, including the on-axis and transverse directions as well as any off-axis direction. Secondly, the transformed strain components acting on the corresponding crack surfaces in each ply of a laminate are considered in the model formulation. This allows the model to account for any general multiaxial strain state. The transformed strain components were ultimately utilized to define the effective strains, which were then used to define the constraint parameters. This is a key contribution in this study since the effects of multiaxiality were added directly into the constitutive equations. It should be emphasized here that the transformed strains acting normal to a crack surface, and not the applied strains, must be used in the model formulation since they contribute to the COD. Moreover, the laminate constitutive equations were reformulated by segregating the different damage modes. This has allowed for the definition of a set of damage constants for each damage mode for a specific laminate. As a result, the SDM model can now accurately capture the nonlinear stiffness degradation, and can be applied to any general symmetric laminate containing multiple distinct damage modes. Finally, the constraint parameters, which account for the coupling effect between the different damage modes, are not assumed to be constant. They are in fact dependent on the evolving ply crack densities, and are represented by continuous inverse sigmoidal functions. This also allows the model to automatically capture the nonlinear stiffness response.

With respect to computational micromechanics, the task of defining a RUC for an arbitrary laminate with a specific damage scenario was also important as this allowed

for the application of periodic boundary conditions on the micromechanical FE models. This was necessary not only to ensure that the FE models provided a proper representation of the physical problem, but also to allow for consideration of the laminate shear response. Since the prediction model accounts for degradation of the in-plane shear modulus (i.e., $a_3, b_3 \neq 0$), nonlinear shear stress-strain behavior can in fact be accounted for. The accuracy of the different laminate RUC micromechanical FE models were in fact validated with theory and experimental data. In addition, the capabilities of the micromechanical models to predict COD, as well as their ability to capture the constraint effects between adjacent plies for various multiaxial strain states was illustrated. This was also key for including multiaxial effects into the SDM prediction model.

The developed multiaxial SDM model was then utilized to predict stiffness degradation for three different classes of laminate configurations involving distinct evolving damage states, and correlations were shown with micromechanical FE prediction data. Although the model accuracy has been demonstrated, development of the current model is still in progress. One assumption made in the formulation of the damage tensor, Eq. (2), and the constraint parameters in the constitutive equations, Eq. (10), was that the CSD (i.e., mode II) had so far been neglected. It is not clear at this stage whether or not addition of the corresponding CSD will greatly influence the stiffness predictions of the SDM model. A study by Varna (2008) has demonstrated that although neglecting CSD in the SDM model formulation may lead to relatively small prediction errors, CSDs may play a critical role in the shear deformation response for particular laminates. This paper is concerned with the extension of the multiscale SDM methodology for multiaxial deformation states, and thus inclusion of CSDs into the formulation is left for a future study.

In addition to the above model limitations, critical damage such as delamination between adjacent plies and fiber fracture is not considered by the current prediction model as its scope has been limited to sub-critical intra-ply matrix cracking. Delamination and fiber fracture have been observed to occur much later than matrix cracking for most practical laminates. Therefore, the SDM model is suitable for predicting stiffness degradation prior to the onset of these critical damage modes. For many practical composite structures, a critical loss in stiffness is sufficient to define failure of a component. It should be noted that if the current model is adopted for predicting failure of a component in the sense that there is a loss of load-bearing capacity, then these critical damage modes must be considered. Again, this is left for a future study.

The presented SDM model can in fact be used to predict evolution of cracks in multidirectional laminates subjected to multiaxial strains if a suitable damage evolution methodology is incorporated. In this study, the damage evolution for multiaxial conditions was assumed in order to showcase the stiffness prediction capabilities of the SDM model. Predicting damage evolution under multiaxial conditions is undoubtedly a very complex task which is lacking in the literature. Damage evolution prediction is addressed by the authors in Montesano and Singh (2015).

Finally, the long-term goal is to utilize the SDM model to predict damage evolution in practical composite components subjected to local multiaxial strains. In order to do so, the analytical SDM model presented here must also be implemented into a commercial FE software package as is described by [Montesano and Singh \(2014\)](#). This is important for predicting the integrity and durability of composite structures, and for designing structures that are damage tolerant and fail-safe. This type of model can also be integrated with a NDE technique for real-time health monitoring of composite structures, which will lead to safer and more cost-effective structures.

6. Conclusions

This paper briefly summarized the development of a synergistic damage mechanics-based model for predicting stiffness degradation in multidirectional laminates containing sub-critical matrix cracks in multiple orientations. The model overcomes the limitations of traditional continuum damage mechanics-based models by utilizing computational micromechanics, in lieu of experimental data, within a multi-scale framework to define the material constants in the constitutive equations. The model is capable of accounting for the effects of multiaxial strain states on the laminate behavior, which was one of the main contributions of this study. This was accomplished by developing a physically accurate representation of the laminate microstructure and by invoking the appropriate periodic boundary conditions in the corresponding computational FE models. As a result, the model is now capable of predicting the shear deformation response of composite laminates. Furthermore, since the model is based on a three-dimensional representation of the laminate microstructure, it accurately captures the constraint effects between adjacent plies within the laminate. Therefore, the prediction model is more robust and is suitable for predicting stiffness degradation for any symmetric laminate containing any number of multidirectional damage modes subjected to any arbitrary multiaxial strain state. This is seen as an advantage when compared to existing models reported in the literature. It is also worth noting that the model can easily be implemented into a commercial finite element software to predict stiffness degradation in composite structures.

The predicted stiffness results were shown to correlate well with the experimental data and with the computational FE data, which provides support for the capabilities of the prediction model. It should however be noted that the model is not fully developed at this stage. First, the inclusion of crack surface sliding displacement in the model and its influence on stiffness predictions must be investigated. Although the SDM model currently does not consider crack sliding for stiffness predictions, the micromechanical FE models can determine these displacements and will be used in a future study. Secondly, the model currently does not consider compressive damage modes. This would also have to be investigated if the model were to be invoked to predict stiffness degradation of practical composite structures.

Acknowledgments

The authors would like to thank the Natural Sciences and Engineering Research Council (NSERC) of Canada and the University of Toronto for funding in support of this work.

References

- Allen, D.H., Harris, C.E., Groves, S.E., 1987. A thermomechanical constitutive theory for elastic composites with distributed damage – I: Theoretical development. *Int. J. Solids Struct.* 23, 1301–1318.
- Chamis, C.C., Abdi, F., Garg, M., Minnetyan, L., Baird, H., Huang, D., Housner, J., Talagani, F., 2013. Micromechanics-based progressive failure analysis prediction for WWFE-III composite coupon test cases. *J. Compos. Mater.* 47, 2695–2712.
- Dvorak, G.J., Laws, N., Hejazi, M., 1985. Analysis of progressive matrix cracking in composite laminates. 1. Thermoelastic properties of a ply with cracks. *J. Compos. Mater.* 19, 216–234.
- Flatscher, T.H., Schuecker, C., Pettermann, H.E., 2013. A constitutive ply model for stiffness degradation and plastic strain accumulation: its application to the third world wide failure exercise (part A). *J. Compos. Mater.* 47, 2575–2593.
- Hashin, Z., 1985. Analysis of cracked laminates: a variational approach. *Mech. Mater.* 4, 121–136.
- Highsmith, A.L., Reifsnider, K., 1982. Stiffness-reduction mechanisms in composite laminates. In: Reifsnider, K. (Ed.), *Damage in Composite Materials*. ASTM STP 775, Philadelphia, pp. 103–117.
- Kaddour, A.S., Hinton, M.J., Smith, P.A., Li, S., 2013. The background to the third world-wide failure exercise. *J. Compos. Mater.* 47, 2417–2426.
- Kashtalyan, M., Soutis, C., 2013. Predicting residual stiffness of cracked composite laminates subjected to multi-axial inplane loading. *J. Compos. Mater.* 47, 2513–2524.
- Ladeveze, P., LeDantec, E., 1992. Damage modeling of the elementary ply for laminated composites. *Compos. Sci. Technol.* 43, 257–267.
- Laurin, F., Carrere, N., Huchette, C., Marie, J.F., 2013. A multiscale hybrid approach for damage and final failure predictions of composite structures. *J. Compos. Mater.* 47, 2713–2747.
- Li, S., Singh, C.V., Talreja, R., 2009. A representative volume element based on translational symmetries for FE analysis of cracked laminates with two arrays of cracks. *Int. J. Solids Struct.* 46, 1793–1804.
- Lomov, S.V., Ivanov, D.S., Verpoest, I., Zako, M., Kurashiki, T., Nakai, H., Hirose, S., 2007. Meso-FE modelling of textile composites: road map, data flow and algorithms. *Compos. Sci. Technol.* 67, 1870–1891.
- Mayugo, J.A., Camanho, P.P., Maimi, P., Davila, C.G., 2010. Analytical modeling of transverse matrix cracking of $[\pm\theta/90_n]_s$ composite laminates under multiaxial loading. *Mech. Adv. Mater. Struct.* 17, 237–245.
- McCartney, L.N., 1998. Predicting transverse crack formation in cross-ply laminates. *Compos. Sci. Technol.* 58, 1069–1081.
- Montesano, J., Singh, C.V., 2014. Progressive failure analysis of polymer composites using a synergistic damage mechanics methodology. In: *Proceedings of the 143rd TMS Annual Meeting & Exhibition*, San Diego, US, Feb. 16–20.
- Montesano, J., Singh, C.V., 2015. Predicting evolution of ply cracks in composite laminates subjected to biaxial loading. *Compos. Part B*. submitted for publication.
- Nairn, J.A., 1989. Strain energy release rate of composite microcracking: a variational approach. *J. Compos. Mater.* 23, 1106–1129.
- Singh, C.V., 2013. A higher order synergistic damage model for prediction of stiffness changes due to ply cracking in composite laminates. *Comput. Mater. Continua* 34, 227–249.
- Singh, C.V., Talreja, R., 2009. A synergistic damage mechanics approach for composite laminates with matrix cracks in multiple orientations. *Mech. Mater.* 41, 954–968.
- Singh, C.V., Talreja, R., 2010. Evolution of ply cracks in multidirectional composite laminates. *Int. J. Solids Struct.* 47, 1338–1349.
- Singh, C.V., Talreja, R., 2013. A synergistic damage mechanics approach to mechanical response of composite laminates with ply cracks. *J. Compos. Mater.* 47, 2475–2501.
- Talreja, R., 1985. Transverse cracking and stiffness reduction in composite laminates. *J. Compos. Mater.* 19, 355–375.
- Talreja, R., 1994. Damage characterization by internal variables. In: Talreja, R. (Ed.), *Damage Mechanics of Composite Materials*. Elsevier, Amsterdam, pp. 53–78.
- Talreja, R., 1996. A synergistic damage mechanics approach to durability of composite materials systems. In: Cardon, A., Fukuda, H., Reifsnider,

- K. (Eds.), 2012. *Progress in Durability Analysis of Composite Systems*. A.A. Balkema, Rotterdam, pp. 117–129.
- Talreja, R., Singh, C.V., 2012. *Damage and Failure of Composite Materials*. Cambridge University Press, London, ISBN 9780521819428.
- Tong, J., Guild, F.J., Ogin, S.L., Smith, P.A., 1997. On matrix crack growth in quasi-isotropic laminates – I. Experimental investigation. *Compos. Sci. Technol.* 57, 1527–1535.
- Varna, J., 2008. Physical interpretation of parameters in synergistic continuum damage mechanics model for laminates. *Compos. Sci. Technol.* 68, 2592–2600.
- Varna, J., Joffe, R., Akshantala, N.V., Talreja, R., 1999. Damage in composite laminates with off-axis plies. *Compos. Sci. Technol.* 59, 2139–2147.
- Varna, J., Joffe, R., Talreja, R., 2001. A synergistic damage mechanics analysis of transverse cracking in $[\pm\theta/90_4]_s$ laminates. *Compos. Sci. Technol.* 61, 657–665.
- Vyas, G.M., Pinho, S.T., 2012. Computational implementation of a novel constitutive model for multidirectional composites. *Comput. Mater. Sci.* 51, 217–224.